Journal of Constructional Steel Research 160 (2019) 16–22

Contents lists available at ScienceDirect

Journal of Constructional Steel Research

Efficient 3D lateral analysis of cold-formed steel buildings

Nicholas P. Franklin [a,*], Aziz Ahmed [a], Lip H. Teh [b], Emma E. Heffernan [a], Timothy J. McCarthy [b]

[a] ARC Research Hub for Australian Steel Manufacturing, University of Wollongong, Wollongong, Australia
[b] School of Civil, Mining and Environmental Engineering, University of Wollongong, Australia

ARTICLE INFO

Article history:
Received 9 April 2019
Received in revised form 23 May 2019
Accepted 23 May 2019
Available online 30 May 2019

Keywords:
3D building analysis
Cold-formed steel building
Equivalent shear modulus
Lateral behaviour
System behaviour
Shell element

ABSTRACT

Non-structural components contribute significantly to the lateral stiffness of a cold-formed steel (CFS) building structure, but are cumbersome to model explicitly in the structural analysis. They are therefore commonly ignored in a 3D structural analysis, and their benefits are lost to the design. This paper proposes an efficient modelling method that enables practical and accurate 3D elastic analysis of a multi-storey CFS building structure to study its lateral behaviour within the serviceability limit state. Each shear or gravity wall is represented by an equivalent shear modulus four-node orthotropic shell element, which incorporates the lateral stiffness (or flexibility) contributions of all components including sheathing, braces and fasteners as present in the wall. The equivalent shear modulus is determined from the experimental test of a representative wall panel, or from the analysis of a finely detailed finite element model of the panel. The resulting two-storey building model, which has much fewer degrees of freedom compared to conventional models, is verified against full-scale shake table test results with respect to the natural period, the peak storey drift and the peak floor acceleration at two different construction phases. This paper demonstrates that the proposed modelling method not only saves analysis time considerably through the drastic reduction of degrees of freedom, but also compares favourably against a published modelling method in terms of accuracy and modelling efforts.

1. Introduction

Cold-formed steel (CFS) members are increasingly used as primary structural components in building systems around the world. However, in Australia the use of CFS members for load bearing applications in mid-rise buildings has been extremely limited. Improvements to the analysis and design procedures in terms of efficiency and accuracy, and better understanding of the sway behaviour of CFS buildings could lead to greater uptake in the construction industry. The ability to incorporate the contributions of non-structural components to the lateral resistance of a CFS building will also be beneficial.

The lateral load resisting system of a CFS building generally comprises either strap-braced [6] or sheathed shear walls [11]. Currently, CFS lateral load resisting design codes require the shear walls to take the entire lateral load themselves. This requirement does not take into account the stiffening effect of non-structural wall sheathing and other components which are essential for fire and acoustic compliance.

Within the timber industry in the USA, full-scale building testing has been carried out [15] resulting in improvements to design standards and modelling methods. Since then, full-scale tests of CFS building structures were undertaken in China [14], Italy [8] and at the University at Buffalo, USA, as a part of the National Science Foundation funded Network for Earthquake Engineering Simulation (NEES) project: CFS-NEES [21]. The NEES project involved full-scale two storey shake table tests of a CFS building at its different construction phases. The fully completed building's response was up to 16 times stiffer than that of the earlier construction, which was without non-structural components [12]. This result demonstrates the significant and beneficial effect of non-structural components, and highlights the importance of modelling non-structural components in the structural analysis.

A number of studies have developed various methods to model CFS shear wall behaviour, with a focus on seismic response. Shear walls in CFS building structures are commonly sheathed with Oriented Strand Board (OSB), which is rigid in plane while the wall panel deforms through the flexibility of the sheathing connections. This behaviour has been replicated by Buonopane et al. [2] with the shear walls being modelled using a rigid diaphragm attached to nonlinear spring elements simulating the fasteners. Bian et al. [1] extended this research, using the model to analyse shear and gravity wall systems. A number of other studies have used a similar method involving the modelling of shear wall connections [1,2,5,7,19,23,25]. This fastener-based method can accurately simulate the behaviour of a shear wall but involves a large number of degrees of freedom which may be impractical for full-scale multi-storey building simulations, and may not be applicable to strap braced shear walls.

To simplify the modelling of shear wall behaviour, shear wall panels have been modelled using linear frame elements and

* Corresponding author.
E-mail address: nf932@uowmail.edu.au (N.P. Franklin).

https://doi.org/10.1016/j.jcsr.2019.05.029
0143-974X/

nonlinear diagonal braces as an equivalent truss [7,9,10,13,22]. Fülöp and Dubina [9] developed a trilinear hysteretic model using frame elements to simulate single shear walls. Leng et al. [12] produced a number of models of varying fidelity using OpenSees for the CFS NEES building with the characterisation of nonlinear behaviour for shear walls, gravity walls, interior walls, and semi-rigid floor and roof diaphragms. Wall components were modelled taking into account the pinching effect in the hysteretic response on the basis of design equations and sub-system level tests. Leng et al. [12] extended the use of equivalent beam column elements by modelling sheathing subpanels. Li et al. [14] created a shear wall model based on the restoring force of wall fasteners, represented as an equivalent bracing. This method has reduced degrees of freedom compared to the fastener-based method, however many elements are still required for each wall in the building.

Further simplification of the shear wall representation has been developed by Martínez-Martínez and Xu [18] with the use of a 16-node equivalent modulus shell element model without hold-downs. The equivalent modulus is a representation of the sheathing and stud properties. A three-storey building was modelled using this method, and the results for lateral displacements compared favourably against a conventional FEA model. However, no comparisons were made against laboratory test results.

This paper proposes the use of an equivalent shear modulus four-node orthotropic shell element to model each wall for the purpose of simulating the elastic sway behaviour of a CFS multi-storey building, incorporating the lateral stiffness contributions of shear walls as well as non-structural components. The FE modelling herein will focus on accurately simulating the elastic stiffness of the system with a view to facilitating the serviceability limit state design of CFS mid-rise buildings under lateral loading such as wind.

The advantages of the proposed modelling method are twofold. First, it can be used whether the sheathing is OSB, gypsum or steel sheeting, and it can even be used for strap-braced shear walls. Second, it is significantly more efficient than the existing modelling methods [1,2,7,9,10,12,14,19,22,23,25]. A bibliography of proposed numerical models can be found in a recent paper by Usefi et al. [24].

Due to the absence of quasi-static tests, the resulting building model will be verified against the results of shake table tests undertaken at low level seismic excitations [21], with respect to the natural period, peak storey drift and peak floor acceleration. Analyses will be taken at two different construction phases in order to demonstrate the lateral stiffness contributions of gravity walls and their elements.

2. Methodology

2.1. Shear and gravity walls

This paper uses an equivalent shear modulus four-node orthotropic shell element to model each of the CFS shear and gravity walls. Fig. 1 depicts a four-node shell element of height h and width b, modelling a wall of the same dimension. The thickness t of the shell element is the same as that of the wall. The deflection of the shell element (i.e. wall) under a horizontal load F is also depicted in the figure, where δ_s is the deflection due to shear deformation of the shell element and δ_{HD} is the upward deflection of the hold-down. A hold-down is an anchorage device used to hold down the bottom track at the chord stud's location.

The total deflection δ_T of the shell element is given in Eq. (1) where k_T is the total lateral stiffness

$$\delta_T = \delta_S + \frac{h}{b}\delta_{HD} = \frac{F}{k_T} \tag{1}$$

The hold-down deflection δ_{HD} is equal to

$$\delta_{HD} = \frac{\frac{h}{b}F}{k_{HD}} \tag{2}$$

in which the k_{HD} is the stiffness of the hold-down.

The deflection δ_s due to shear deformation is given by Eq. (3) where G_{XZ} is the equivalent (in-plane) shear modulus of the shell element

$$\delta_S = \frac{Fh}{G_{xz}tb} \tag{3}$$

Eqs. (2) and (3) are substituted into Eq. (1) to give the equivalent shear modulus

$$G_{xz} = \frac{h}{\left(\frac{tb}{k_T} - \frac{th^2}{bk_{HD}}\right)} \tag{4}$$

The total stiffness k_T can be obtained from a laboratory test using Eq. (1), as illustrated in Section 3.1. Alternatively, it can also be obtained from the analysis of a finely detailed finite element model of the wall panel.

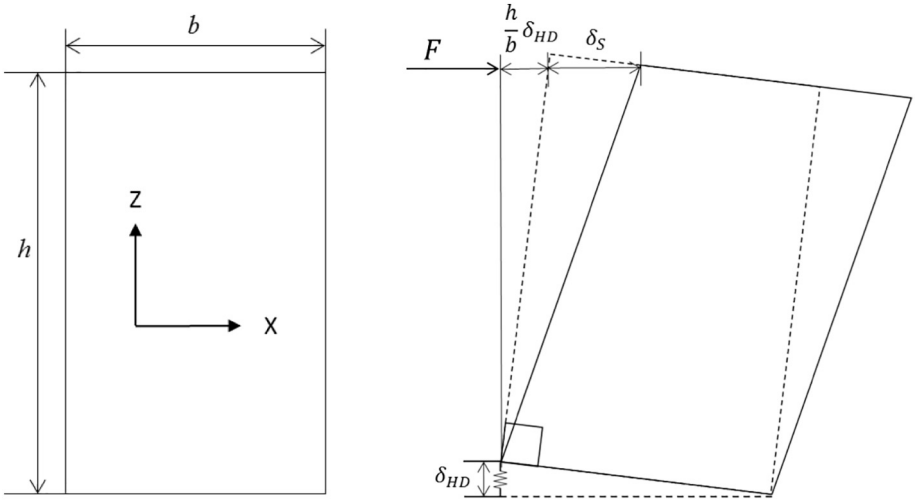

Fig. 1. Shell element geometry and deflections.

2.2. Hold-downs

Hold-downs are modelled using spring and gap link elements at the two base nodes of the shell element. Hold-downs have a very high stiffness in compression, which is simulated by the gap element. The gap element is massless and is assigned a high stiffness of 10^7 kN/mm in the Z direction. In tension, the spring acts with a constant stiffness of 9.93 kN/mm for the shear wall analysed in the present work [13]. The hold-downs for gravity walls are modelled with one tenth of the stiffness of the shear wall hold-downs [1]. Shear anchors are not modelled as the hold-downs are restrained in the horizontal directions.

3. Verification

To verify the proposed methodology, a two-storey building [21] was modelled in ETABS at two construction phases, and the analysis results were compared with the experimental data and the beam-column analysis results of Leng [13] for the natural period, peak storey drift and peak floor acceleration (Phase 1: A1-3D-SDa, Phase 2b: A2b-3D-SDa). Shake table test results were used for verification due to the lack of quasi-static tests of full scale CFS buildings.

3.1. Tested wall stiffness values

The wall stiffness values were derived from the shear and unsheathed gravity wall tests undertaken as part of the CFS-NEES project [16]. The tested components had construction details consistent with those used in the full-scale shake table test [21]. The experimental shear wall specimen with OSB sheathing is shown in Fig. 2.

A number of CFS wall types were subjected to monotonic and cyclic loading under displacement control [16]. The specimens were 2.74 m high and 1.22 m or 2.44 m long, with either OSB sheathing, gypsum sheathing or no sheathing. The walls were framed with 600S162-54 studs and S/HDU6 hold-downs with a specified stiffness of 9.93 kN/mm. In the current study, the stiffness was estimated at a deflection equal to the highest expected deflection of the full-scale building when tested under low level seismic excitation [20]. The total stiffnesses k_T of the 1.22 and 2.44 m long OSB sheathed shear walls with ledger were found to be 0.785 and 2.47 kN/mm, respectively [17].

3.2. CFS NEES shake table test

Shake table testing was undertaken for a full-scale two storey CFS framed building as part of the CFS-NEES project [21]. The building was designed using the allowable strength method for a location in Orange County, California. The specimen was 7 m by 15.2 m in plan and 5.8 m in height. There were several CFS shear walls and gravity walls with and without window openings. OSB sheathed CFS joist floor and roof panels were used in a ledger framing system. The shear walls utilised back-to-back chord studs, and were designed as laterally decoupled, requiring a hold-down at both ends of each wall segment. Simpson Strong-Tie S/HDU6 hold-downs were used at the base of the shear walls on the ground floor. Steel straps were used to transfer horizontal forces from the upper to the lower chords.

Fig. 2. Experimental specimen with OSB sheathing (Source: [16]).

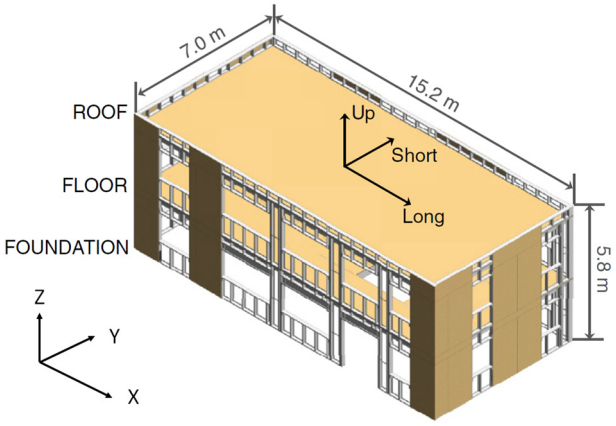

Fig. 3. Phase 1 isometric drawing (Source: [12]).

Testing was undertaken at a number of different construction phases aiming to quantify the effects of non-structural components on the building's structural performance. In this paper, two of the phases are analysed, denoted as Phase 1 and Phase 2b.

Phase 1 consisted mainly of structural elements only: single-sided OSB sheathed shear walls, roof, floor and unsheathed gravity walls, as illustrated in Fig. 3. Phase 2b had the addition of exterior OSB sheathing on the gravity walls (i.e. sheathed on one side only). However, the two phases were designed to have similar total weights on the shake table through the use of supplemental concrete blocks and steel plates. The only (primary) variable affecting the frame's responses under shaking was therefore the system stiffness.

Table 1 details the construction differences between the two phases. The framing labels can be explained through an example of the ground floor shear wall; 600S162-54. '600' is the web depth in 100th inches, 'S' refers to stud or joist section, '162' is the flange width expressed in 100th inches and '54' is the minimum base metal thickness in 1000th inches. Field stud refers to any stud that is not a chord stud.

Two ground motion records of the 1994 Northridge earthquake were used in the tests [21] at a number of scaling levels, being from the Canoga Park and the Rinaldi receiving stations as provided by the Pacific Earthquake Engineering Research Center (PEER). The unscaled ground motions are shown in Fig. 4, while the actual peak accelerations analysed in the present work are given in Table 2. As indicated in the

Table 1
Construction details for Phase 1 and Phase 2b buildings.

	Framing	Phase 1	Phase 2b
		OSB	OSB
Floor diaphragm	Joist: 1200S200-97	●	●
Roof diaphragm	Joist: 1200S200-54	●	●
Shear wall 1	Chord: 2 × 600S162-54 Field: 600S162-54	●	●
Shear wall 2	Chord: 2 × 600S162-54 Field: 600S162-53	●	●
Gravity wall 1	600S162-54	○	●
Gravity wall 2	600S162-33	○	●
Interior wall	362S162-54	○	○

● = OSB present; ○ = OSB absent.

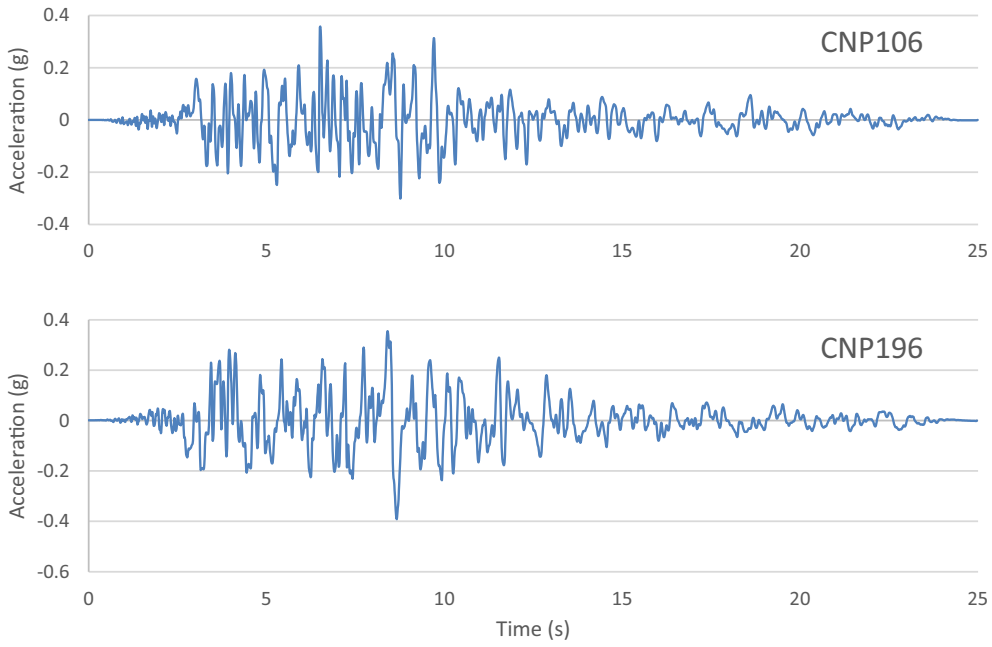

Fig. 4. Unscaled ground motions CNP106 and CNP196.

Table 2
Seismic record data.

PEER record	CNP106	CNP196
Direction	Y	X
Axis	Short	Long
Actual phase 1 excitation PGA (g)	0.061	0.083
Actual phase 2b excitation PGA (g)	0.061	0.085

table, different ground motions were applied in the short and long directions.

In the present work, the natural period was determined using free vibration analysis in ETABS [4]. To determine the peak storey drift and the peak floor acceleration, nonlinear time history analysis was used. Analyses were undertaken using factored seismic records to match the actual Phase 1 and Phase 2b Peak Ground Acceleration from the shake table tests [20].

3.2.1. Modelling walls, floor and roof

Fig. 5 shows the present building model in ETABS, with the blue colour denoting shear walls and the grey colour, gravity walls. In the tests, chord studs were connected between storeys with a steel strap, which was modelled in the present work by using a shared node between the upper and the lower shell elements.

The shear moduli for various lengths of shear walls in the building were determined through interpolation between the 1.22 and 2.44 m wide shear walls obtained from the laboratory tests [17]. For the sheathed gravity walls, due to the absence of laboratory tests, the elastic stiffness was assumed to be the same as the OSB sheathed shear walls.

Sheathed gravity walls with openings naturally have a reduced stiffness. As there is no test data available for such walls, the shear modulus of a wall with an opening is factored by the square root of the proportion of the wall area that is sheathed. For example, a wall with a 55% sheathed area has a shear modulus equal to 74% of that of a fully sheathed wall that was tested [17]. It will not be appropriate to linearly factor the shear modulus as an opening is typically located centrally within the wall, without reducing the wall width.

The vertical elastic modulus of the shell element E_Z was initially assumed to be 5 GPa as it was around the typical value for OSB panels [3]. However, the value can also be justified through the concept of effective shell areas in compression and tension due to overturning moment. An effective area is the area on either the windward or leeward side of the shell element that has an equivalent axial resistance to the

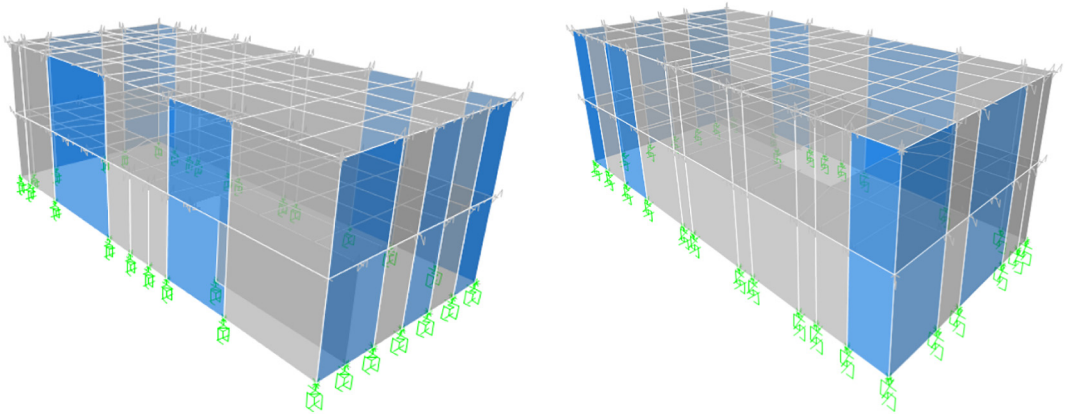

Fig. 5. Opposing views of 3D building model in ETABS.

Table 3
Phase 1 wall components.

Component	t (mm)	G_{XZ} (MPa)	E_Z (GPa)	Mass (kg/m^3)
Shear wall 1	164	17.9–24.9	5	116
Shear wall 2	164	17.9–24.9	5	116
Gravity wall 1	152	0.3	2.7	77
Gravity wall 2	152	0.3	2.7	34
Interior wall	92	0.5	2.7	65

Table 4
Phase 2b wall components.

Component	t (mm)	G_{XZ} (MPa)	E_Z (GPa)	Mass (kg/m^3)
Shear wall 1	164	17.9–24.9	5	116
Shear wall 2	164	17.9–24.9	5	116
Gravity wall 1	152	19.3–28.1	2.7	103
Gravity wall 1 – opening	152	14.3–20.8	2.7	103
Gravity wall 2	152	14.4–21.1	2.7	56
Gravity wall 2 – opening	152	10.7–15.6	2.7	56
Interior wall	92	0.5	2.7	65

Table 5
Seismic masses.

	Phase 1 (kg)	Phase 2b (kg)
Roof	13,370	13,384
Floor	18,949	19,263

A damping ratio of 5% was assumed in all analyses.

chord stud. For a 164 mm thick shear wall with back-to-back 600S162-54 chord studs, the effective width is equal to 157 mm, which the authors consider reasonable. For the gravity wall with a single 600S162-54 stud as an end post, used in the shake table test [17], the vertical elastic modulus is equal to 2.7 GPa for the same effective width. For both shear and gravity walls, the horizontal elastic modulus is assumed to be 500 MPa, or one tenth of the vertical elastic modulus of a shear wall as the wall's horizontal stiffness does not benefit from the presence of studs.

Tables 3 and 4 list the properties of the wall components of Phases 1 and 2b, respectively.

For simplicity, parapets were not explicitly modelled, but their mass was accounted for as described in the next paragraph. The floor and roof were modelled as rigid diaphragms using four-node shell elements that correspond to the wall panel edges. Due to the ledger framing system, the joints between the floor and the walls are assumed to be pinned.

The masses of the walls, floor and roof were modelled in ETABS through the use of elemental mass and additional mass. Elemental mass is the self-weight of the components. The elemental masses of the shell elements are determined by calculating the mass per volume based on the information provided by Peterman [20]. In calculating the wall mass for Phase 2b, it was assumed there were no openings, so the weight was distributed evenly throughout each wall type.

Table 6
Phase 1 first mode natural periods.

Direction	Test [21] (s)	Present (s)	Leng [13] (s)
X – long	0.32	0.32 (0%)	0.30 (−6%)
Y – short	0.36	0.36 (0%)	0.32 (−11%)

Table 7
Phase 2b first mode natural periods.

Direction	Test [21] (s)	Present (s)	Leng [13] (s)
X – long	0.20	0.21 (+5%)	0.22 (+10%)
Y – short	0.30	0.32 (+7%)	0.28 (−7%)

Additional masses representing the parapet and dummy concrete blocks were then applied as a surface load in ETABS, equal to that in the testing [20]. The seismic masses of the roof and floor in Phases 1 and 2b are given in Table 5.

3.2.2. Results

The first mode natural periods were determined for both the long (X) and the short (Y) directions. Fig. 6 depicts the first mode shapes.

The first mode natural periods found in the shake table tests and the analyses are shown in Tables 6 and 7 for Phases 1 and 2b, respectively. The percentages in brackets denote the analysis deviations from the test results.

It can be seen that the present analysis results are closer to the test results than Leng's [13] for both construction phases. Both models were able to simulate the significant decreases in the natural periods due to the increased building lateral stiffness from Phase 1 to Phase 2b, reflecting the effects of gravity walls and their elements.

Each peak storey drift was determined by averaging the corresponding displacements of the four corner nodes and dividing the result by the storey height. The X displacement was measured under seismic excitation in the long direction (CNP196), and the Y displacement was measured under excitation in the short direction (CNP106). Due to the small magnitude and susceptibility to random noise, the displacement in the perpendicular direction of each excitation is not considered. Fig. 7 shows the present analysis results for the lower storey drift in Phase 1.

The peak storey drifts are shown in Tables 8 and 9 for Phases 1 and 2b, respectively. The percentages in brackets denote the analysis deviations from the test results. Drift time history results were not compared with the test data as the latter was not available.

Table 8 shows that the accuracy of the present model for the peak storey drifts in Phase 1 is not so good as for the natural periods in the same phase, but is better than the beam-column model of Leng [13].

In Phase 2b the present model's results for the upper storey's peak storey drifts deviated more from the shake table test results compared to the model of Leng [13], as shown in Table 9. For the lower storey, the present model's peak storey drifts remained reasonably accurate.

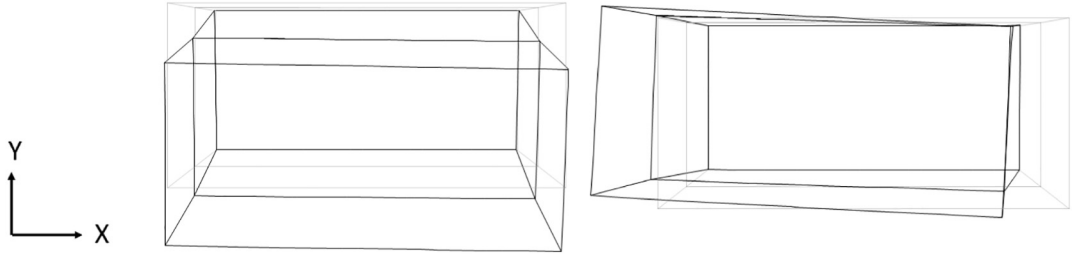

Fig. 6. First mode of vibration in the short and long directions.

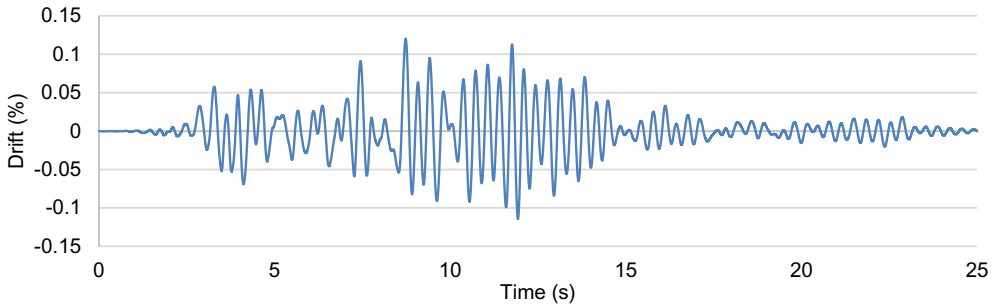

Fig. 7. Phase 1 lower storey drift in the long direction.

Table 8
Phase 1 peak storey drifts.

Direction	Storey	Test [21] (drift %)	Present (drift %)	Leng [13] (drift %)
X – long	Lower	0.12	0.12 (0%)	0.10 (−17%)
Y – short	Lower	0.10	0.09 (−10%)	0.08 (−20%)
X – long	Upper	0.11	0.09 (−18%)	0.03 (−73%)
Y – short	Upper	0.08	0.07 (−13%)	0.04 (−50%)

Table 9
Phase 2b peak storey drifts.

Direction	Storey	Test [21] (drift %)	Present (drift %)	Leng [13] (drift %)
X – long	Lower	0.04	0.04 (0%)	0.10 (+150%)
Y – short	Lower	−0.08	0.09 (+13%)	0.12 (+50%)
X – long	Upper	−0.04	0.02 (−50%)	0.05 (+25%)
Y – short	Upper	−0.06	0.08 (+33%)	−0.05 (−17%)

Table 10
Phase 1 peak floor acceleration.

Direction	Diaphragm	Test [21] (g)	Model (g)	Leng [13] (g)
X – long	Floor	0.142	0.100 (−30%)	0.170 (+20%)
Y – short	Floor	0.085	0.078 (−8%)	0.224 (+164%)
X – long	Roof	0.177	0.170 (−4%)	0.179 (+1%)
Y – short	Roof	0.125	0.145 (+16%)	0.228 (+82%)

It is uncertain why the present model's deviation for the upper storey is as high as 50%, although the use of only 1 significant figure was likely a factor.

Each peak floor (or roof) acceleration was determined by averaging the accelerations of the four corner nodes in the relevant direction, expressed as a fraction of the gravity acceleration. The peak accelerations of the floor and roof are shown in Tables 10 and 11 for Phases 1 and 2b, respectively.

The deviations from the test results of the present analysis results for the peak floor accelerations are relatively large compared to the results for the natural periods, but are much smaller than those of Leng [13]. It appears that peak floor accelerations are more sensitive to modelling assumptions than natural periods and peak storey drifts.

The deviations in peak floor accelerations of the present analysis results could also be due to the seismic input that might not exactly represent the shake table tests. The seismic data used in the present analyses were obtained from the ground motion records shown in Fig. 4 and Table 2 and scaled to match the peak test input. On the other hand, during the shake table tests, there were likely to be deviations from the intended seismic input.

Table 11
Phase 2b peak floor acceleration.

Direction	Diaphragm	Test [21] (g)	Model (g)	Leng [13] (g)
X – long	Floor	0.106	0.092 (−13%)	0.431 (+307%)
Y – short	Floor	0.079	0.094 (+19%)	0.630 (+697%)
X – long	Roof	0.133	0.156 (+17%)	0.398 (+199%)
Y – short	Roof	0.119	0.187 (+57%)	0.884 (+643%)

4. Conclusions

This paper has presented an efficient modelling method for practical 3D elastic analysis of a multi-storey cold-formed steel building that incorporates the lateral stiffness contributions of non-structural shear components such as gravity walls and their elements. It represents each wall with an equivalent shear modulus four-node orthotropic shell element, drastically reducing the number of degrees of freedom and therefore the analysis time. The entailed modelling efforts are also significantly less compared to the conventional frame modelling method.

Verification of the resulting building model against published shake table test results of a two-storey building prototype found that the proposed modelling method was able to account for the lateral stiffness contributions of gravity walls and their elements, and compared favourably against a published modelling method in terms of accuracy with respect to the natural periods, the peak storey drifts and the peak floor accelerations at two different construction phases.

Acknowledgements

The authors would like to thank the Australian Research Council for funding this research through the ARC Research Hub for Australian Steel Manufacturing under the Industrial Transformation Research Hubs scheme (Project ID: IH130100017). The authors would also like to thank the Sustainable Building Research Centre at the Innovation Campus of the University of Wollongong for the use of its facilities.

References

[1] G. Bian, D.A. Padilla-Llano, S.G. Buonopane, C.D. Moen, B.W. Schafer, OpenSees modeling of wood sheathed cold-formed steel framed shear walls, Structural Stability Research Council Annual Stability Conference 2015, SSRC 2015, (July) 2015, pp. 219–232.
[2] S.G. Buonopane, T.H. Tun, B.W. Schafer, Fastener-based computational models for prediction of seismic behavior of CFS shear walls, 10th U.S. National Conference on Earthquake Engineering: Frontiers of Earthquake Engineering, NCEE 2014, 2014.
[3] Z. Cai, R.J. Ross, Mechanical Properties of Wood-Based Composite Materials, U.S. Dept. of Agriculture, Forest Service, Forest Products Laboratory, Madison, WI, 2010 , Available at: http://www.fpl.fs.fed.us/documnts/fplgtr/fplgtr190/chapter_12.pdf.
[4] Computers and Structures Inc, Structural Software for Building Analysis and Design | ETABS, Available at https://www.csiamerica.com/products/etabs 2015.
[5] F. Derveni, S. Gerasimidis, K.D. Peterman, Capturing cold-formed steel shear wall behavior through nonlinear fastener- based modeling, Proceedings of the Annual Stability Conference Structural Stability Research Council April 2–5. St. Louis, Missouri, 2019.
[6] T.S. Eom, T.H. Ha, B.H. Cho, T.H. Kim, Cyclic loading tests on framed stud walls with strap braces and steel sheathing, J. Struct. Eng. 141 (7) (2015), 04014173.
[7] L. Fiorino, S. Shakeel, V. Macillo, R. Landolfo, Seismic response of CFS shear walls sheathed with nailed gypsum panels: numerical modelling, Thin-Walled Struct. 122 (April 2017) (2018) 359–370.

[8] L. Fiorino, V. Macillo, R. Landolfo, Shake table tests of a full-scale two-story sheathing-braced cold-formed steel building, Eng. Struct. 151 (2017) 633–647 , Available at https://doi.org/10.1016/j.engstruct.2017.08.056.
[9] L.A. Fülöp, D. Dubina, Performance of wall-stud cold-formed shear panels under monotonic and cyclic loading - part II: numerical modelling and performance, Thin-Walled Struct. 42 (2) (2004) 321–338.
[10] S. Kechidi, N. Bourahla, Deteriorating hysteresis model for cold-formed steel shear wall panel based on its physical and mechanical characteristics, Thin-Walled Struct. 98 (2016) 421–430 , Available at https://doi.org/10.1016/j.tws.2015.09.022.
[11] F. Lam, G.L. Helmut, M. He, Lateral resistance of wood shear walls with large sheathing panels, J. Struct. Eng. 123 (12) (1994) 1666–1673.
[12] J. Leng, K.D. Peterman, G. Bian, S.G. Buonopane, B.W. Schafer, Modeling seismic response of a full-scale cold-formed steel-framed building, Eng. Struct. 153 (2017) 146–165 , Available at https://doi.org/10.1016/j.engstruct.2017.10.008.
[13] J. Leng, Simulation of Cold-Formed Steel Structures, Johns Hopkins University, 2015.
[14] Y. Li, R. Ma, Z. Shen, Numerical simulation on dynamic behavior of a cold-formed steel framing building test model, 22nd International Specialty Conference on Cold-Formed Steel Structures, 2014 , Available at http://scholarsmine.mst.edu/isccss/22iccfss/session12/2.
[15] J.W. van de Lindt, S.E. Pryor, S. Pei, Shake table testing of a full-scale seven-story steel–wood apartment building, Eng. Struct. 33 (3) (2011) 757–766.
[16] P. Liu, K.D. Peterman, B.W. Schafer, Impact of construction details on OSB-sheathed cold-formed steel framed shear walls, J. Constr. Steel Res. 101 (2014) 114–123 , Available at http://www.sciencedirect.com/science/article/pii/S0143974X14001382.
[17] P. Liu, K.D. Peterman, B.W. Schafer, Test Report on Cold-Formed Steel Shear Walls, 2012.
[18] J. Martínez-Martínez, L. Xu, Simplified nonlinear finite element analysis of buildings with CFS shear wall panels, J. Constr. Steel Res. 67 (4) (2011) 565–575 , Available at https://doi.org/10.1016/j.jcsr.2010.12.005.
[19] S.E. Niari, B. Rafezy, K. Abedi, Seismic behavior of steel sheathed cold-formed steel shear wall: experimental investigation and numerical modeling, Thin-Walled Struct. 96 (2015) 337–347 , Available at https://doi.org/10.1016/j.tws.2015.08.024.
[20] K. Peterman, Behaviour of full-scale cold-formed steel buildings under seismic excitations, Johns Hopkins University, 2014 , Available at https://www.cambridge.org/core/product/identifier/S0007125000277040/type/journal_article.
[21] B.W. Schafer, D. Ayhan, L. Leng, et al., Seismic response and engineering of cold-formed steel framed buildings, Structures 8 (2016) 197–212.
[22] I. Shamim, C.A. Rogers, Steel sheathed/CFS framed shear walls under dynamic loading: numerical modelling and calibration, Thin-Walled Struct. 71 (2013) 57–71 , Available at https://doi.org/10.1016/j.tws.2013.05.007.
[23] Y. Telue, M. Mahendran, Behaviour and design of cold-formed steel wall frames lined with plasterboard on both sides, Eng. Struct. 26 (5) (2004) 567–579.
[24] N. Usefi, P. Sharafi, H. Ronagh, Numerical models for lateral behaviour analysis of cold-formed steel framed walls: state of the art, evaluation and challenges, Thin-Walled Struct. 138 (2019) 252–285.
[25] X. Zhou, Y. He, Y. Shi, T. Zhou, Y. Liu, Experiment and Fe analysis on shear resistance of cold-formed steel stud assembled wall in residential structure, Adv. Steel Constr. 6 (3) (2010) 914–925.